



# Performance comparison of different flow arrangements of 4-fluid internally-cooled liquid desiccant dehumidifiers

Ali Pakari<sup>1</sup> · Saud Ghani<sup>1</sup>

Received: 18 July 2021 / Accepted: 17 February 2022 / Published online: 14 March 2022  
© The Author(s) 2022

## Abstract

In this study, the performance of 10 different flow arrangements of 4-fluid internally-cooled liquid desiccant dehumidifiers were compared. The four fluids are supply air, exhaust air, liquid desiccant, and water. The comparison was performed using a two-dimensional heat and mass transfer model of the dehumidifier that was solved numerically. The model's predictions of supply air outlet humidity ratio matched experimental measurements within 6.7%. The two-dimensional variation of the air temperature and humidity ratio in the supply channel showed the importance of using a two-dimensional heat and mass transfer model when at least one of the fluids is in cross-flow with the other fluids. Moreover, a sensitivity analysis was performed to evaluate the effect of nine input parameters (supply air temperature and humidity ratio, exhaust air temperature and humidity ratio, liquid desiccant temperature, concentration, and flow rate, supply air mass flow rate, and exhaust to supply air mass flow rate ratio) on the performance of the dehumidifiers. The results showed that the best performance, in terms of the supply air humidity ratio and enthalpy decrease, was obtained when the supply air was in counter-flow with the exhaust air, liquid desiccant, and water. While the poorest performance was obtained when the supply air was in parallel-flow with the exhaust air and in counter-flow with the liquid desiccant and water. The approximate difference between the best and poorest performing flow arrangements in terms of the decrease in supply air humidity ratio and enthalpy is 4.3% and 10.5%, respectively. The results of the sensitivity analysis showed that for the 10 flow arrangements, the liquid desiccant inlet temperature, and flow rate have the least effects on the performance of the dehumidifier.

**Keywords** Heat and mass transfer · Flow type · Liquid desiccant · Dehumidification · Numerical model · Enthalpy change

## Abbreviations

$C_{LD}$	Liquid desiccant concentration, $\text{kg}_{\text{salt}} \text{kg}_{\text{solution}}^{-1}$	$L$	Channel length, m
$C_p$	Specific heat, $\text{J kg}^{-1} \text{K}^{-1}$	$\dot{M}$	Mass flow rate, $\text{kg s}^{-1}$
$d_h$	Hydraulic diameter, m	$\dot{m}$	Mass flow rate per channel, $\text{kg s}^{-1}$
$D_{\text{membrane}}$	Membrane diffusivity, $\text{m}^2 \text{s}^{-1}$	Nu	Nusselt number
$D_{\text{va}}$	Mass diffusivity of water vapor in air, $\text{m}^2 \text{s}^{-1}$	$P_{\text{atm}}$	Atmospheric pressure, Pa
$h$	Enthalpy, $\text{kJ kg}^{-1}$	$P_g$	Saturated vapor pressure, Pa
$H$	Convective heat transfer coefficient, $\text{W m}^{-2} \text{K}^{-1}$	$P_{LD}$	Saturated vapor pressure above the liquid desiccant, Pa
$h_{\text{dilution}}$	Enthalpy of dilution of aqueous solutions of lithium chloride, $\text{J kg}^{-1}$	$r$	Exhaust air-to-supply air mass flow rate ratio
$h_{\text{fg}}$	Enthalpy of evaporation of water, $\text{J kg}^{-1}$	Sh	Sherwood number
$h_m$	Mass transfer coefficient, $\text{m s}^{-1}$	$T$	Temperature, °C
$k$	Thermal conductivity, $\text{W m}^{-1} \text{K}^{-1}$	$t$	Thickness, mm
		$U$	Overall heat transfer coefficient, $\text{W m}^{-2} \text{K}^{-1}$
		$U_m$	Overall mass transfer coefficient, $\text{kg m}^{-2} \text{s}^{-1}$
		$V$	Volume flow rate, $\text{mL min}^{-1}$
		$v$	Volume flow rate per channel, $\text{mL min}^{-1}$
		$W$	Channel width, m
		$x, y$	Space coordinates

✉ Ali Pakari  
alipakari@outlook.com; ali.pakari@qu.edu.qa

<sup>1</sup> Department of Mechanical and Industrial Engineering,  
College of Engineering, Qatar University, P.O. Box 2713,  
Doha, Qatar

**Greek letters**

$\rho$	Density, $\text{kg m}^{-3}$
$\omega$	Humidity ratio, $\text{kg kg}_{\text{dry air}}^{-1}$

**Subscripts**

e	Exhaust channel
in	Inlet
LD	Liquid desiccant
out	Outlet
s	Supply channel
wf	Water film

**Introduction**

The use of heating and air conditioning systems in buildings is on the rise [1], this has led to an increase in the buildings sector's share of energy consumption and  $\text{CO}_2$  emissions [2], which has led to studying different methods to improve the use of alternative sources of energy [3, 4]. Therefore, the use of environmentally friendly and energy-efficient alternatives to the vapor compression air conditioning systems is becoming increasingly more important. A promising alternative is an air conditioning system that consists of an evaporative cooling system and a liquid desiccant-based dehumidifier. Liquid desiccant dehumidifiers are either adiabatic or internally cooled [5]. It has been shown that the moisture removal rate of an internally-cooled liquid desiccant dehumidifier can be higher by up to 47% [6] and 54% [7] relative to an adiabatic liquid desiccant dehumidifier.

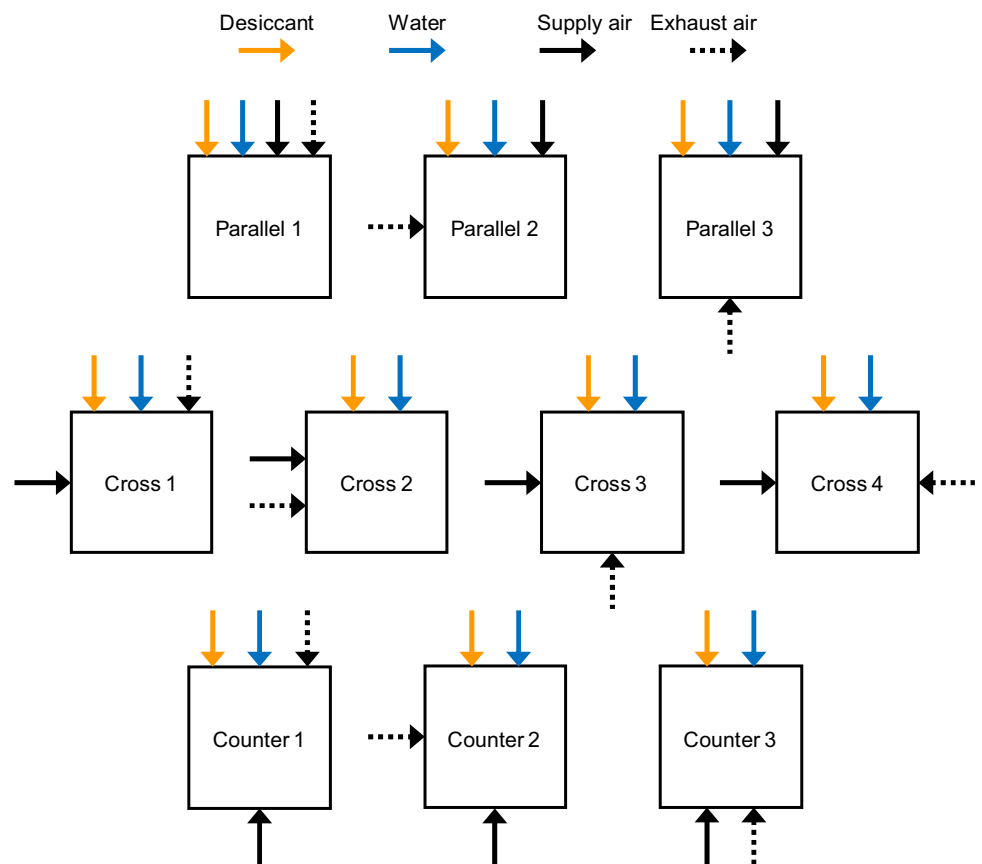
Internally-cooled liquid desiccant dehumidifiers include 3-fluid [8, 9] and 4-fluid designs [10–12]. The three fluids in a 3-fluid design are supply air, liquid desiccant, and a coolant (chilled water or refrigerant). The dehumidifier is a compact heat and mass exchanger that consists of a stack of channels. Supply air and liquid desiccant flow in the supply channels, while chilled water flows in the exhaust channels. The 4-fluid design is a liquid desiccant dehumidifier with internal evaporative cooling, the four fluids are supply air, liquid desiccant, exhaust air, and water. Similar to the 3-fluid design, the dehumidifier consists of supply and exhaust channels. Supply air and liquid desiccant flow in the supply channels, where the dehumidification takes place, while exhaust air and water flow in the exhaust channels, where the evaporative cooling takes place.

Heat and mass exchangers are typically classified according to flow arrangement and it is well known that their performance is dependent on the flow arrangement. A number of studies [13–17] have been conducted to compare the performance of different flow arrangements of 3-fluid internally-cooled liquid desiccant dehumidifiers. Liu et al. [13] analyzed the performance of 6 flow arrangements of 3-fluid internally-cooled liquid desiccant dehumidifiers

using a two-dimensional (2D) heat and mass transfer model. The three fluids were supply air, liquid desiccant, and cooling water. It was concluded that the two flow arrangements where the supply air and liquid desiccant are in counter-flow have the best performance, the cooling water was in cross-flow and in counter-flow with the supply air in these two flow arrangements. Liu et al. [14] compared the performance of 3-fluid internally-cooled liquid desiccant dehumidifiers with 10 different flow arrangements. The three fluids were supply air, liquid desiccant, and cooling water. The comparison was performed using a heat and mass transfer model of the dehumidifier. The study concluded that, for best performance, the supply air should be in counter-flow with the cooling water and in cross-flow with the liquid desiccant. Li and Yao [15] analyzed the performance of 10 different flow arrangements of 3-fluid internally-cooled liquid desiccant dehumidifiers. The three fluids were supply air, liquid desiccant, and cooling water. The comparison was performed using a heat and mass transfer model of the dehumidifier. It was shown that the best dehumidification performance was obtained when the supply air was in counter-flow with the liquid desiccant and cooling water. In another study, using the same model, Li and Yao [16] compared the performance of 10 different flow arrangements of 3-fluid internally-cooled liquid desiccant dehumidifiers in terms of cooling capacity. It was concluded that the highest cooling capacity is obtained when the supply air flows in cross-flow with the liquid desiccant and in counter-flow with the cooling water. Using a 2D heat and mass transfer model, Guan et al. [17] compared the performance of 3 flow arrangements of 3-fluid internally-cooled liquid desiccant systems. The three fluids were supply air, liquid desiccant, and refrigerant. In the first flow arrangement, the air and liquid desiccant flow in parallel-flow. In the second flow arrangement, the air and liquid desiccant flow in cross-flow, and in the third flow arrangement, the air and liquid desiccant flow in counter-flow. Considering the combined performance of the dehumidifier and the regenerator, it was concluded that the counter-flow arrangement showed the best performance.

Although there are few studies that compared the performance of different flow arrangements of 3-fluid internally-cooled liquid desiccant dehumidifiers, to the best knowledge of the authors, no study has compared the different flow arrangements of 4-fluid internally-cooled liquid desiccant dehumidifiers. Therefore, a comparison of the thermal performance of 10 flow arrangements of 4-fluid internally-cooled liquid desiccant dehumidifiers is performed in this study. The 10 flow arrangements of a 4-fluid internally-cooled liquid desiccant dehumidifier considered in this study are shown in Fig. 1. In all flow arrangements, the liquid desiccant and water flow from the top to bottom. The flow arrangements are named according to the flow directions of the supply air and liquid desiccant. For example, in the flow

**Fig. 1** Schematic showing the 10 different flow arrangements of 4-fluid internally-cooled liquid desiccant dehumidifiers



arrangements parallel 1–3, both the supply air and liquid desiccant enter the dehumidifier at the same end and move in the same direction, while the flow direction of the exhaust air, with respect to the supply air, changes from parallel-flow, parallel 1, to cross-flow, parallel 2, and to counter-flow, parallel 3.

This study has two objectives, the first and main objective is to compare 10 flow arrangements of 4-fluid internally-cooled liquid desiccant dehumidifiers in terms of the supply air humidity ratio change and supply air enthalpy change. The second objective is to evaluate the effect of nine input parameters, namely supply air temperature and humidity ratio, exhaust air temperature and humidity ratio, liquid desiccant temperature, concentration, and flow rate, supply air mass flow rate, and exhaust to supply air mass flow rate ratio, on the performance of the 10 flow arrangements of 4-fluid liquid desiccant dehumidifiers. The comparison is conducted using a 2D model of the heat and mass transfer in 4-fluid liquid desiccant dehumidifiers. The model is validated by comparing its predictions to experimental measurements from literature.

The remainder of this paper is structured as follows. ‘[Experimental](#)’ gives a brief description of the experimental setup, including the specifications of the prototype and the test conditions. ‘[Numerical model](#)’ presents the heat

and mass transfer model, including the governing equations, boundary conditions, and transfer coefficients. In ‘[Results and discussion](#)’, the results are presented and discussed. Finally, the conclusions of the study are presented in ‘[Conclusions](#)’.

## Methods

### Experimental

The experiments conducted by Woods and Kozubal [11] were used to validate the numerical heat and mass transfer model. A brief description of the dehumidifier used in conducting the experiments is as follows. The core of the dehumidifier was a heat exchanger that consisted of a stack of 36 pairs of supply and exhaust channels. Schematic of a channel pair is shown in Fig. 2. As shown in the figure, the supply air and liquid desiccant flow in cross-flow, with the supply air flowing left to right (horizontal) and the liquid desiccant (lithium chloride) flowing from top to bottom (vertical direction). While the exhaust air and water flow in parallel-flow, both flow vertically from top to bottom. The specifications of the dehumidifier are listed in Table 1. To ensure the uniform

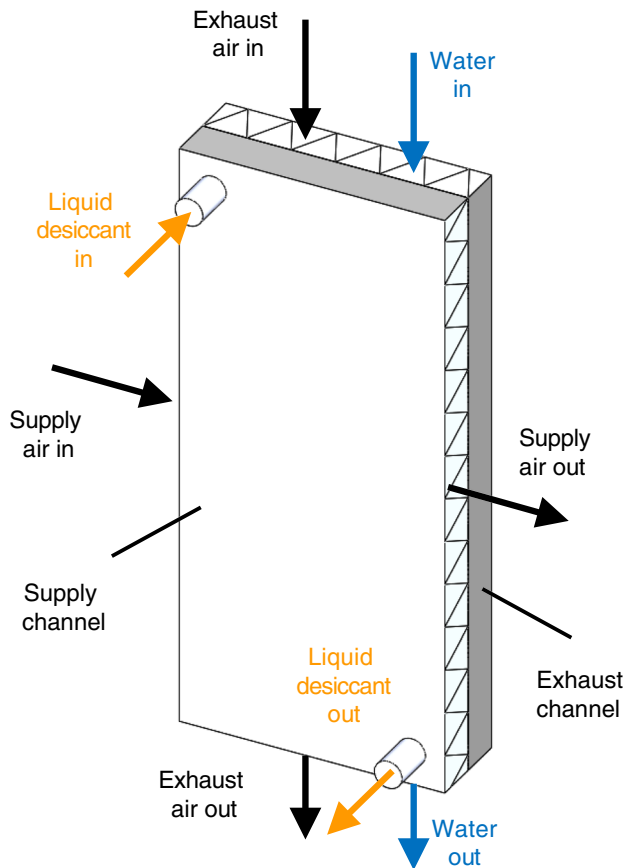


Fig. 2 Schematic of a pair of supply and exhaust channels

Table 1 Specifications of the dehumidifier

Parameter	Symbol	Value	Unit
Supply channel thickness	$t_s$	3.175	mm
Exhaust channel thickness	$t_e$	3.175	mm
Channel length	$L$	0.24	m
Channel width	$W$	0.535	m
Plate thickness	$t_{\text{plate}}$	0.4	mm
Wick thickness	$t_{\text{wick}}$	0.3	mm
Membrane thickness	$T_{\text{membrane}}$	20	$\mu\text{m}$
Membrane diffusivity	$D_{\text{membrane}}$	1.48e-6	$\text{m}^2 \text{s}^{-1}$
Membrane thermal conductivity	$k_{\text{membrane}}$	0.06	$\text{W m}^{-1} \text{K}^{-1}$

distribution of liquid desiccant and water, the walls of the supply and exhaust channels were covered with wicking material. In the supply channels, membranes were attached on the wicking material. The dehumidifier was tested by varying the inlet conditions of the supply air,

exhaust air, and liquid desiccant. The test conditions are listed in Table 2 [11].

## Numerical model

Figure 3 shows a schematic of a pair of supply and exhaust channels having the flow arrangement of cross 1, as shown in Fig. 1. This flow arrangement is selected for presenting the heat and mass transfer model since it has the same flow arrangement as the experimental setup. The supply air flows in the positive  $x$  direction, in cross-flow with respect to the exhaust air and liquid desiccant, which are flowing in the negative  $y$  direction. It should be noted that according to the flow arrangement of the dehumidifier, the governing equations and the corresponding boundary conditions will slightly change. In order to simplify the governing equations, the following assumptions are made [18, 19]:

1. The system is insulated; therefore, no heat transfer occurs between the device and the surroundings.
2. The thickness of the channels is small relative to the channel length and width; therefore, the variations of temperature and humidity ratio normal to the flow are neglected, reducing the problem to be two-dimensional.
3. The flow is incompressible, laminar, fully developed, and steady.
4. The mass flow rates are constant.
5. The heat and mass transfer coefficients are constant.
6. Heat and mass transfer analogy holds.

## Heat and mass transfer governing equations

By applying the stated assumptions, the differential equations that govern the heat and mass transfer in the internally-cooled liquid desiccant dehumidifier are given as follows. In these equations, subscripts  $s$ ,  $e$ , LD, and  $wf$  refer to the supply channel, exhaust channel, liquid desiccant, and water film, respectively.

Energy balance of the supply air is given by

$$\dot{m}_s C_{p,s} \frac{\partial T_s}{\partial x} = UW(T_{LD} - T_s), \quad (1)$$

where  $U$  is the overall heat transfer coefficient, determined by

$$U = \left( \frac{1}{H_s} + \frac{t_{\text{membrane}}}{k_{\text{membrane}}} \right)^{-1}, \quad (2)$$

where  $H$  is the convective heat transfer coefficient,  $t_{\text{membrane}}$  is the thickness of the membrane, and  $k_{\text{membrane}}$  is the thermal conductivity of the membrane.

Energy balance of the exhaust air is given by

**Table 2** Experimental test conditions [11]

Test no.	$T_{s,in}/^{\circ}\text{C}$	$\omega_{s,in}/\text{kg kg}^{-1}$	$T_{e,in}/^{\circ}\text{C}$	$\omega_{e,in}/\text{kg kg}^{-1}$	$\dot{M}_s/\text{kg s}^{-1}$	$\dot{M}_e/\text{kg s}^{-1}$	$T_{LD,in}/^{\circ}\text{C}$	$C_{LD}/\text{kg kg}^{-1}$	$V_{LD}/\text{mL min}^{-1}$
1	20.9	0.0146	–	–	0.152	–	31.4	0.380	337
2	20.9	0.0146	–	–	0.106	–	29.0	0.383	310
3	20.9	0.0146	–	–	0.197	–	30.9	0.380	337
4	26.7	0.0146	35.0	0.0186	0.152	0.061	30.4	0.373	337
5	26.7	0.0146	26.7	0.0186	0.152	0.061	31.7	0.375	360
6	26.7	0.0146	26.7	0.0132	0.152	0.061	31.2	0.378	337
7	26.7	0.0146	35.0	0.0132	0.152	0.061	31.1	0.380	337
8	35.0	0.0186	35.0	0.0186	0.152	0.061	34.8	0.385	360
9	26.7	0.0146	35.0	0.0186	0.152	0.046	32.0	0.380	337
10	26.7	0.0146	35.0	0.0186	0.152	0.030	31.3	0.378	337
11	26.7	0.0146	35.0	0.0186	0.106	0.042	32.8	0.381	310
12	26.7	0.0146	35.0	0.0186	0.182	0.073	30.7	0.379	337
13	26.7	0.0146	35.0	0.0186	0.152	0.061	32.9	0.380	337
14	35.0	0.0186	35.0	0.0186	0.152	0.061	38.2	0.424	299
15	44.2	0.0146	35.0	0.0186	0.152	0.061	36.1	0.430	299
16	26.7	0.0146	35.0	0.0186	0.152	0.061	32.2	0.380	583
17	26.7	0.0146	35.0	0.0186	0.152	0.061	25.9	0.330	572
18	26.7	0.0146	35.0	0.0171	0.152	0.061	25.2	0.360	443
19	26.7	0.0146	35.0	0.0146	0.152	0.061	29.3	0.340	515
20	26.7	0.0146	35.0	0.0132	0.152	0.046	30.3	0.340	515

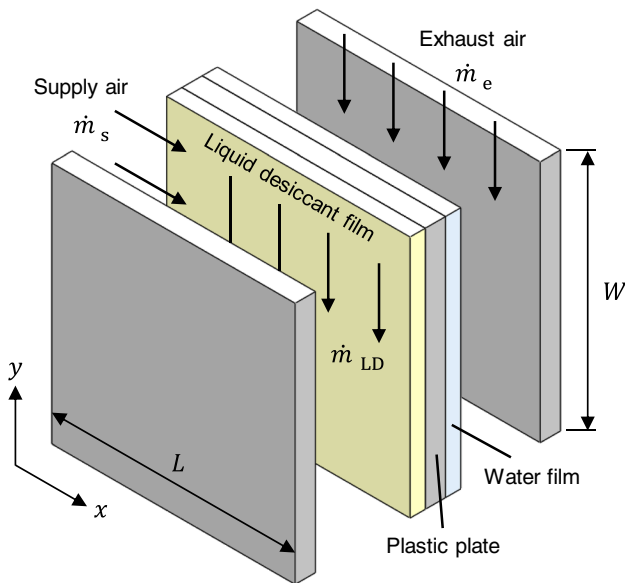


**Fig. 3** Schematic of the dehumidifier used to develop the heat and mass transfer model

$$-\dot{m}_e C_{p,e} \frac{\partial T_e}{\partial y} = H_e L (T_{wf} - T_e). \tag{3}$$

The specific heats of the supply and exhaust air are determined by the following equation [20]:

$$C_p = C_{p,air} + \omega C_{p,vapor}, \tag{4}$$

where  $\omega$  is the humidity ratio,  $C_{p,air}$  ( $1007 \text{ J kg}^{-1} \text{ K}^{-1}$ ) is the specific heat of air, and  $C_{p,vapor}$  ( $1870 \text{ J kg}^{-1} \text{ K}^{-1}$ ) is the specific heat of water vapor at room temperature.

Moisture balance of the supply air is given by

$$\dot{m}_s \frac{\partial \omega_s}{\partial x} = U_{m,s} W (\omega_{LD} - \omega_s), \tag{5}$$

where  $U_{m,s}$  is the overall mass transfer coefficient and  $\omega_{LD}$  is humidity ratio of air in equilibrium with the liquid desiccant film. The overall mass transfer coefficient is calculated using the following equation:

$$U_{m,s} = \left( \frac{1}{H_{m,s} \rho_{air}} + \frac{t_{membrane}}{\rho_{air} D_{membrane}} \right)^{-1} \tag{6}$$

$\omega_{LD}$  is determined by [20]

$$\omega_{LD} = 0.622 \frac{P_{LD}}{P_{atm} - P_{LD}}. \tag{7}$$

The properties of the liquid desiccant solution, including the saturated vapor pressure above the liquid desiccant film,  $P_{LD}$ , density,  $\rho_{LD}$ , thermal conductivity,  $k_{LD}$ , specific heat,  $C_{p,LD}$ , and enthalpy of dilution,  $h_{dilution}$ , are determined by correlations from Conde [21].

Moisture balance of the exhaust air is given by

$$-\dot{m}_e \frac{\partial \omega_e}{\partial y} = H_{m,e} \rho_{\text{air}} L(\omega_{\text{wf}} - \omega_e). \quad (8)$$

The saturated air humidity ratio,  $\omega_{\text{wf}}$ , is determined by Eq. (7), substituting  $P_{\text{LD}}$  with  $P_g$ , the pressure of the saturated vapor at the exhaust air temperature, which is calculated as follows [22, 23]:

$$P_g = (611.21) e^{\left( \left( 18.678 - \frac{T_c}{234.5} \right) \left( \frac{T_c}{257.14 + T_c} \right) \right)}. \quad (9)$$

Energy balance of the liquid desiccant film is given by

$$-\dot{m}_{\text{LD}} C_{p,\text{LD}} \frac{\partial T_{\text{LD}}}{\partial y} + UL(T_{\text{LD}} - T_s) + U_{\text{ms}} L(\omega_{\text{LD}} - \omega_s) (h_{\text{dilution}} + h_{\text{fg}}) + U_{\text{plate}} L(T_{\text{LD}} - T_{\text{wf}}) = 0, \quad (10)$$

where  $h_{\text{dilution}}$  is the enthalpy of dilution of the liquid desiccant and  $h_{\text{fg}}$  is the enthalpy of evaporation of water, which is determined by [24]

$$h_{\text{fg}} = 10^3 (2501 - 2.369 T_{\text{wf}}). \quad (11)$$

The overall heat transfer coefficient of the plastic plate,  $U_{\text{plate}}$ , is calculated as follows:

$$U_{\text{plate}} = \left( \frac{t_{\text{wick}}}{k_{\text{LD}}} + \frac{t_{\text{plate}}}{k_{\text{plate}}} + \frac{t_{\text{wick}}}{k_{\text{wf}}} \right)^{-1}, \quad (12)$$

where  $k_{\text{LD}}$ ,  $k_{\text{plate}}$ , and  $k_{\text{wf}}$  are the thermal conductivity of the liquid desiccant, plastic plate, and water, respectively.

Energy balance of the water film is given by

$$H_e L(T_{\text{wf}} - T_e) + h_{\text{me}} \rho_{\text{air}} L(\omega_{\text{wf}} - \omega_e) h_{\text{fg}} - U_{\text{plate}} L(T_{\text{LD}} - T_{\text{wf}}) = 0. \quad (13)$$

Equations (1), (3), (5), (8), (10), and (13) govern the heat and mass transfer in the internally-cooled liquid desiccant dehumidifier under the stated assumptions.

### Boundary conditions

The governing equations are completed by the following boundary conditions. The inlet conditions of the supply air are specified, Eqs. (14) and (15). At  $y = W$ , the top boundary of the supply channel, the liquid desiccant temperature is specified, Eq. (16). The exhaust air temperature and humidity ratio are specified at the inlet of the exhaust channel, at  $y = W$ , Eqs. (17) and (18).

$$T_s(0, y) = T_{s,\text{in}} \quad (14)$$

$$\omega_s(0, y) = \omega_{s,\text{in}} \quad (15)$$

$$T_e(x, W) = T_{e,\text{in}} \quad (16)$$

$$\omega_e(x, W) = \omega_{e,\text{in}} \quad (17)$$

$$T_{\text{LD}}(x, W) = T_{\text{LD},\text{in}} \quad (18)$$

### Heat and mass transfer coefficients

The convective heat transfer coefficients in the supply and exhaust channels are estimated as follows:

$$H = \frac{Nu k_{\text{air}}}{d_h}. \quad (19)$$

The Nusselt number,  $Nu$ , for parallel plates is assumed to be equal to the average of the constant wall temperature boundary condition (7.541) and constant heat flux (8.235) boundary condition values [25], since the boundary condition at the channel walls is neither constant temperature nor constant heat flux.

The mass transfer coefficient in the supply and exhaust channels are calculated as follows:

$$h_m = \frac{Sh D_{\text{va}}}{d_h}, \quad (20)$$

where  $Sh$  is the Sherwood number, and  $D_{\text{va}}$  is the mass diffusivity of water vapor in air. Given that heat and mass transfer analogy holds, the Sherwood number is considered equal to the Nusselt number.

### Computational grid

The heat and mass transfer equations were discretized and solved using the finite element method. The computational domain, shown in Fig. 4, was discretized using a structured grid with quadrilateral elements. The length and width of the domain were divided into 20 and 40 elements, respectively. The elements along the length and width were distributed using a symmetric arithmetic sequence with an element ratio of 6. The total number of elements in the computational grid is 800. To ensure the selected grid provides grid-independent results, two additional grids with 3200 and 12,800 elements were created. Using the additional two grids, the obtained outlet conditions of the supply air changed by less than 0.1%. Therefore, it was verified that the selected grid provided grid-independent results.



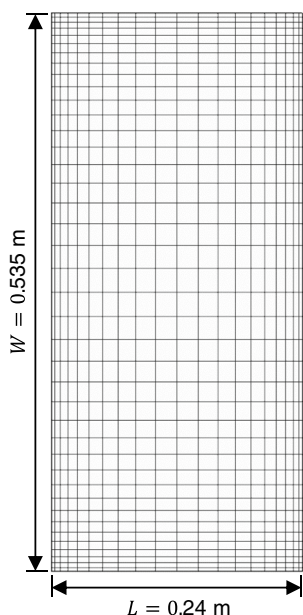


Fig. 4 Computational domain grid

## Results and discussion

### Numerical model validation

To validate the numerical model, the predicted supply air outlet humidity ratio of the experimental tests conditions listed in Table 2 are compared to the measured values [11]. Figure 5 compares the predictions of the numerical model

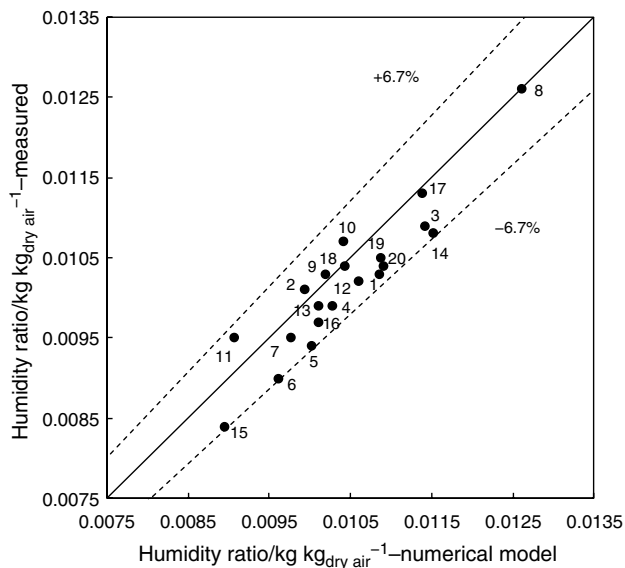


Fig. 5 Numerical model predictions vs experimental measurements of the supply air outlet humidity ratio

with measured values of the supply air outlet humidity ratio. The data labels in the figure represent the test numbers from Table 2. As shown in the figure, the model’s predictions match the measured values within 6.7%. The average difference between the predicted and measured values is about 3.7%. At 16 out of the 20 tests, the model predicted higher outlet humidity ratios compared to the measured values.

### Performance comparison—reference case

Using the test conditions 8 from Table 2 as input conditions, the performance of the 10 flow arrangements of the 4-fluid liquid desiccant dehumidifier is compared in terms of the supply air humidity ratio change,  $\Delta\omega_s (\omega_{s,\text{in}} - \omega_{s,\text{out}})$ , and the supply air enthalpy change,  $\Delta h_s (h_{s,\text{in}} - h_{s,\text{out}})$ . Figure 6a, b shows the supply air humidity ratio change and

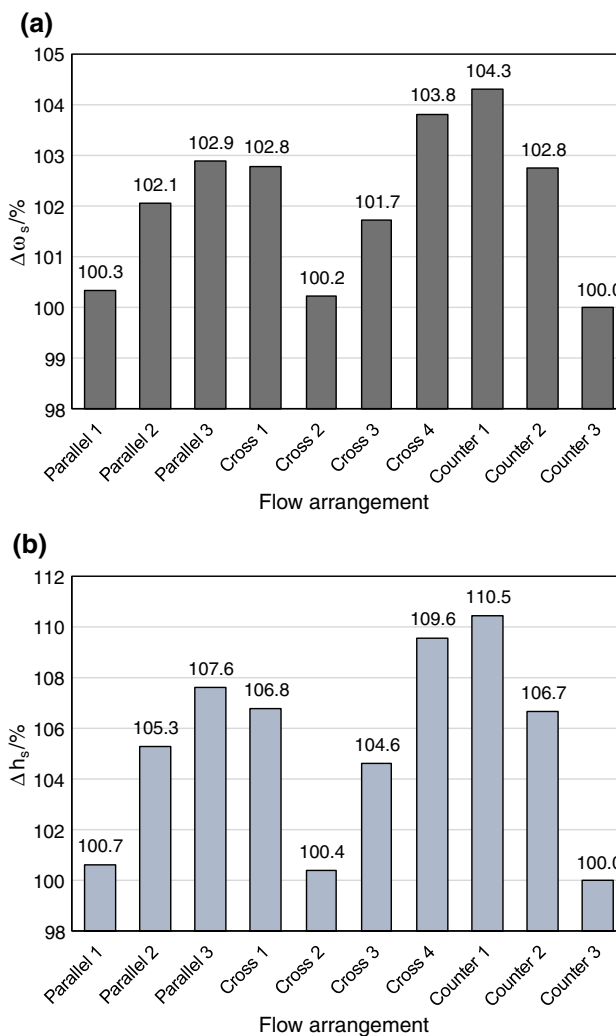


Fig. 6 Comparison of all flow types in terms of a the change in supply air humidity ratio and b the change in supply air enthalpy. The lowest performing flow arrangement, counter 3, is taken as the reference case (100%)

enthalpy change of the 10 flow arrangements in percentage, in which the flow arrangement counter 3 is taken as the reference (100%) since it has the lowest change in supply air humidity ratio and enthalpy.

As shown in Fig. 6a, flow arrangement counter 1 has the highest change in supply air humidity ratio, 104.3%, and enthalpy, 110.5%. The dehumidifiers with the flow arrangements, parallel 1, cross 2, and counter 3, have the lowest performances, in these flow arrangements the supply air and exhaust air are in parallel-flow. While the dehumidifiers with the flow arrangements, parallel 3, cross 4, and counter 1, have the highest performance, in these flow arrangements the supply air and exhaust air are in counter-flow. Therefore, it can be concluded that the flow direction

of the supply and exhaust air with respect to each other has the most effect on the performance.

### Effect of input conditions

In this section, the effect of nine input conditions on the supply air humidity ratio change and supply air enthalpy change are evaluated. In each case the input conditions that are not varied are kept constant and equal to the test conditions 8 from Table 2.

### Effect of supply air inlet temperature

Figure 7 shows the supply air humidity ratio change,  $\Delta\omega_s$ , and the supply air enthalpy change,  $\Delta h_s$ , as functions of the

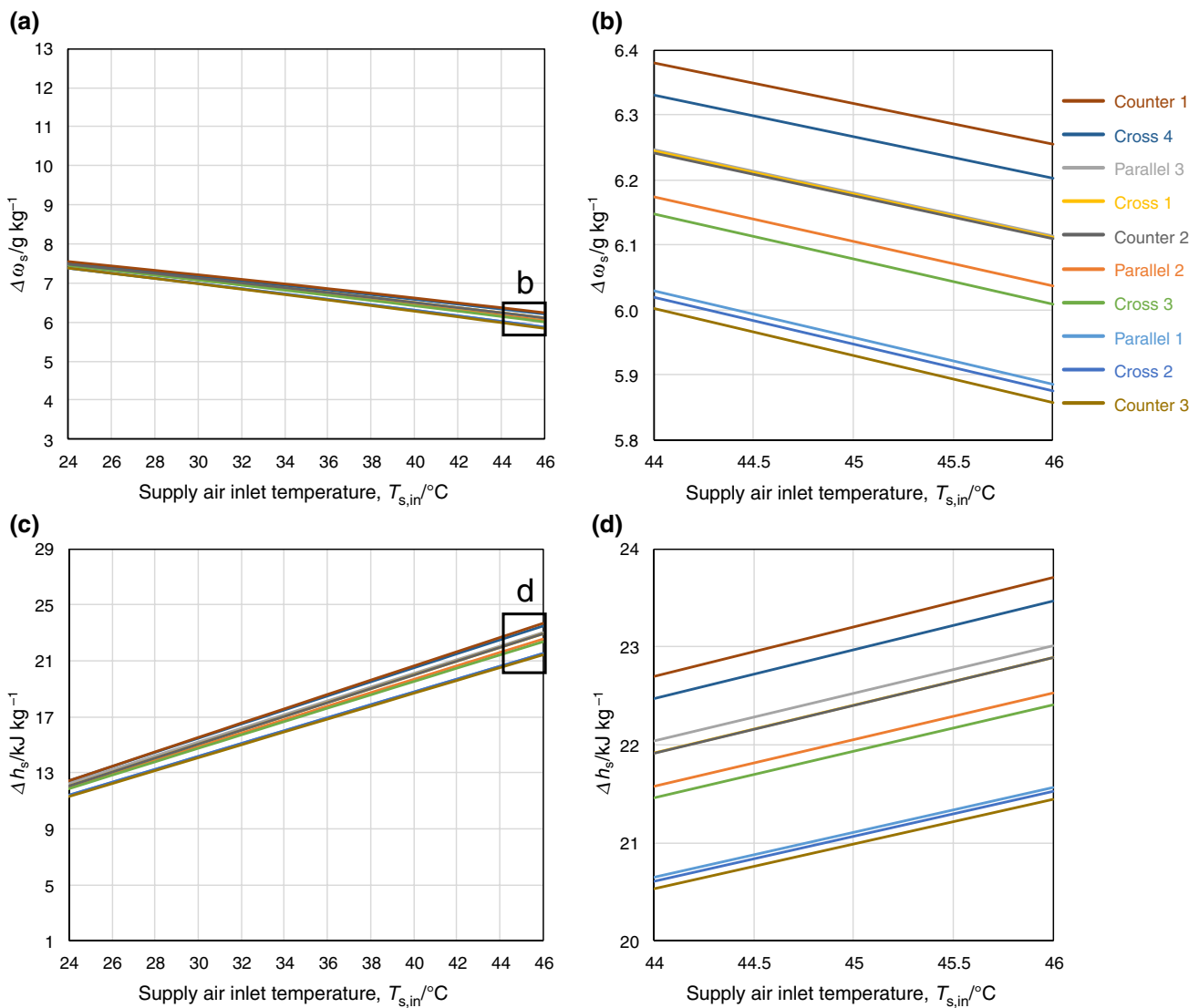


**Fig. 7** The effect of supply air inlet temperature,  $T_{s,in}$ , on **a, b** the humidity ratio change of the supply air and **c, d** the enthalpy change of the supply air for the 10 different flow arrangements of the 4-fluid dehumidifier



supply air inlet temperature,  $T_{s,in}$ , for all 10 flow arrangements. As shown in the figure, increasing the supply air inlet temperature from 24 to 46 °C reduces the change in supply air humidity ratio by about 1.5 g kg<sup>-1</sup> (20%), while it increases the change in supply air enthalpy by about 11 kJ kg<sup>-1</sup> (90%). The respective decrease and increase in the supply air humidity ratio change and enthalpy change can be explained as follows. As the supply air inlet temperature increases, the temperature of the liquid desiccant solution along the dehumidifier increases as well. This increase in temperature leads to an increase in the vapor pressure, and consequently the humidity ratio, of the air in equilibrium with the liquid desiccant, which decreases the dehumidification potential. The difference in performance between the flow arrangements is relatively small; however, as shown in

Fig. 7b, d, which are zoomed-in views of the plots in Fig. 7a, c, it can be noted that the difference in performance between the flow arrangements increases at higher supply air inlet temperatures.

### Effect of supply air inlet humidity ratio

Figure 8 shows the supply air humidity ratio change,  $\Delta\omega_s$ , and the supply air enthalpy change,  $\Delta h_s$ , as functions of the supply air inlet humidity ratio,  $\omega_{s,in}$ , for all 10 flow arrangements. The removed moisture from the supply air increases by about 7 g kg<sup>-1</sup> (140%) and the enthalpy change of the supply air increases by about 14 kJ kg<sup>-1</sup> (100%), by increasing the supply air inlet humidity ratio from 15 to 29 g kg<sup>-1</sup>. Increasing the supply air inlet humidity ratio improves the

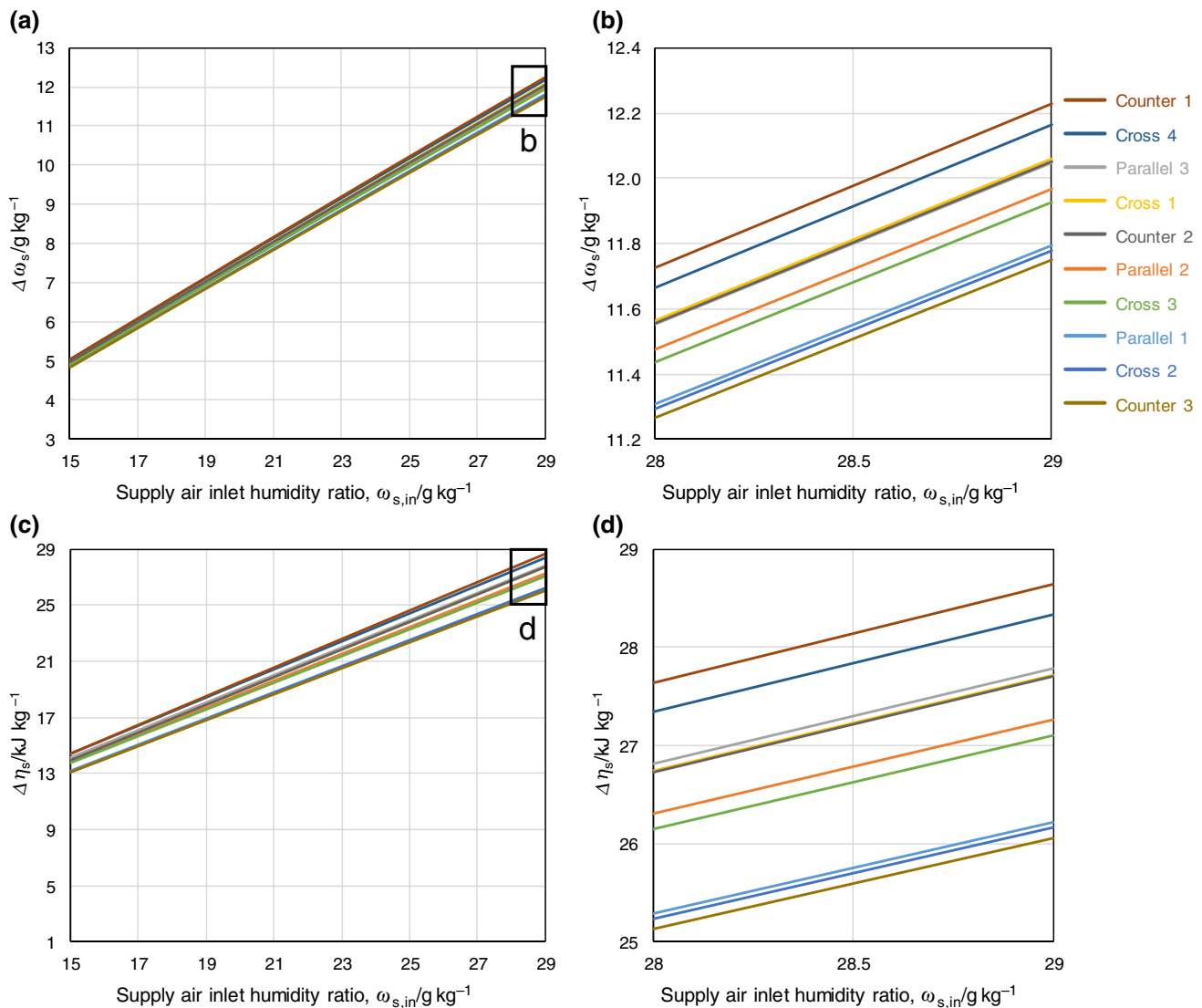


**Fig. 8** The effect of supply air inlet humidity ratio,  $\omega_{s,in}$ , on **a, b** the humidity ratio change of the supply air and **c, d** the enthalpy change of the supply air for the 10 different flow arrangements of the 4-fluid dehumidifier

moisture transfer between the supply air and desiccant solution. The difference in performance between the flow arrangements increases with increasing supply air inlet humidity ratio.

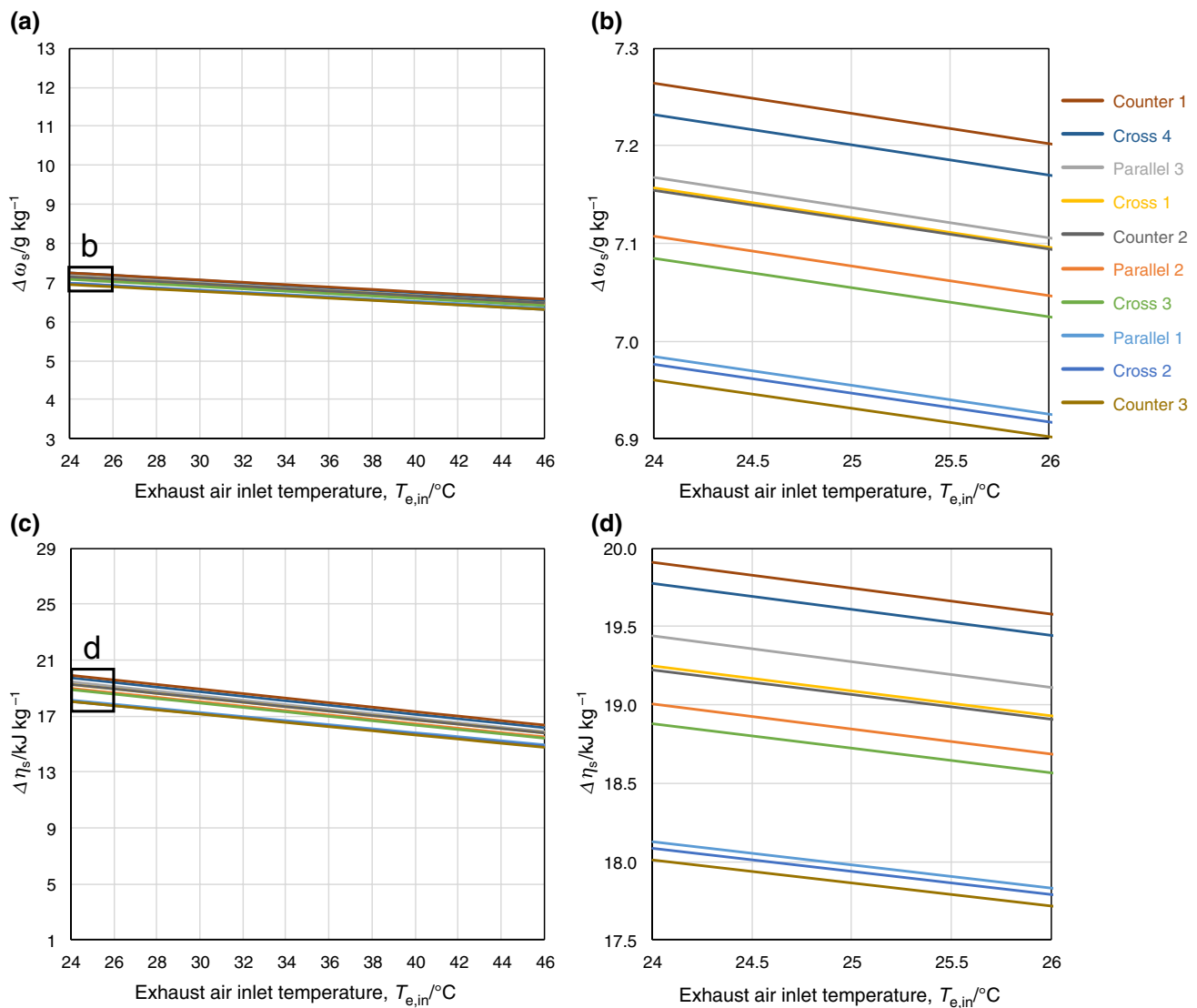
### Effect of exhaust air inlet temperature

Figure 9 shows the supply air humidity ratio change,  $\Delta\omega_s$ , and the supply air enthalpy change,  $\Delta h_s$ , as functions of the exhaust air inlet temperature,  $T_{e,in}$ , for all 10 flow arrangements. Increasing the exhaust air inlet temperature from 24 to 46 °C reduces the change in supply air humidity ratio and enthalpy by about 0.7 g kg<sup>-1</sup> (9.5%) and 3.5 kJ kg<sup>-1</sup> (18%), respectively. Increasing the exhaust air inlet temperature while its humidity ratio is kept constant increases its wet

bulb temperature, which is the lowest attainable temperature in the exhaust channel. Therefore, by increasing the exhaust air temperature, the evaporative cooling potential in the exhaust channel reduces, leading to higher temperatures of the liquid desiccant and consequently lowering the obtained change in the supply air humidity ratio and enthalpy.

### Effect of exhaust air inlet humidity ratio

Figure 10 shows the supply air humidity ratio change,  $\Delta\omega_s$ , and the supply air enthalpy change,  $\Delta h_s$ , as functions of the exhaust air inlet temperature,  $\omega_{e,in}$ , for all 10 flow arrangements. Increasing the exhaust air inlet humidity ratio from 15 to 29 g kg<sup>-1</sup> reduces the change in supply air humidity ratio and enthalpy by about 1 g kg<sup>-1</sup> (14.5%) and 5.3 kJ kg<sup>-1</sup>



**Fig. 9** The effect of exhaust air inlet temperature,  $T_{e,in}$ , on **a, b** the humidity ratio change of the supply air and **c, d** the enthalpy change of the supply air for the 10 different flow arrangements of the 4-fluid dehumidifier

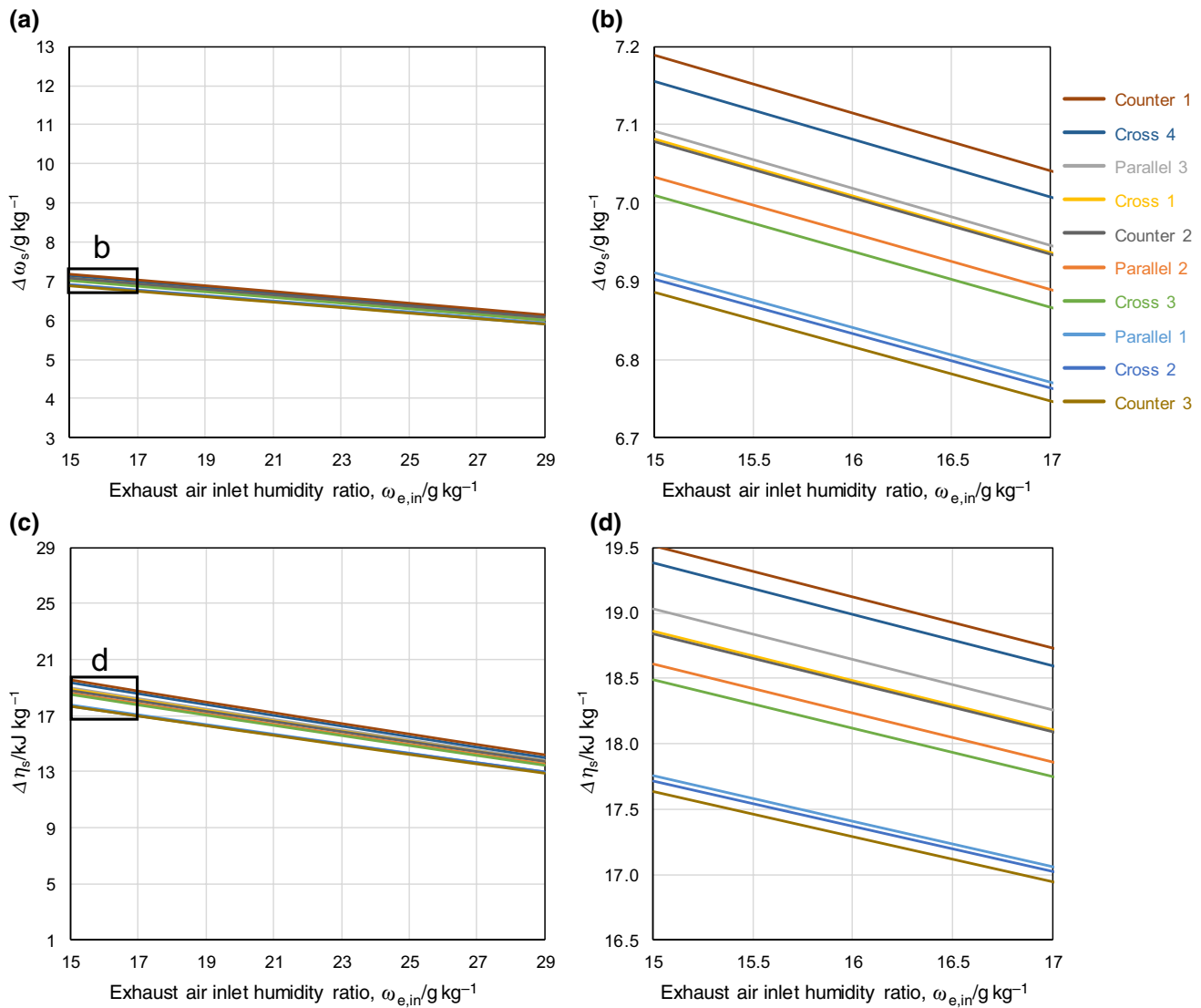


**Fig. 10** The effect of exhaust air inlet humidity ratio,  $\omega_{e,in}$ , on **a, b** the humidity ratio change of the supply air and **c, d** the enthalpy change of the supply air for the 10 different flow arrangements of the 4-fluid dehumidifier

(27%), respectively. Increasing the exhaust air inlet humidity ratio while its temperature is kept constant increases its wet bulb temperature. Therefore, the cooling potential of the exhaust channel is reduced, which leads to higher temperatures of the liquid desiccant and therefore lowering the obtained change in the supply air humidity ratio and enthalpy.

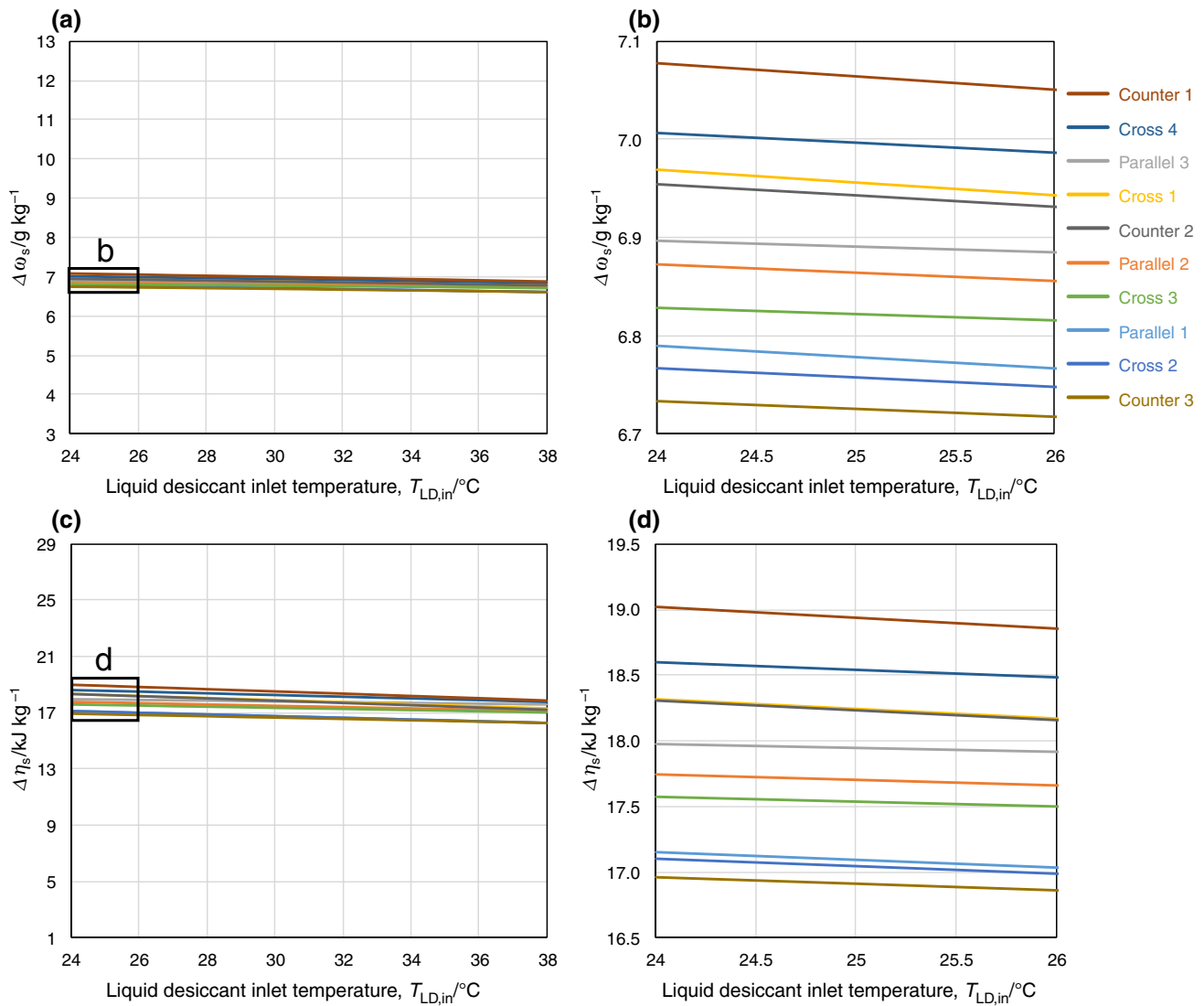
#### Effect of liquid desiccant inlet temperature

Figure 11 shows the supply air humidity ratio change,  $\Delta\omega_s$ , and the supply air enthalpy change,  $\Delta h_s$ , as functions of the liquid desiccant inlet temperature,  $T_{LD,in}$ , for all 10 flow arrangements. Increasing the liquid desiccant inlet temperature from 24 to 38 °C reduces the change in supply air

humidity ratio and enthalpy by about 0.2 g kg<sup>-1</sup> (2.9%) and 1.2 kJ kg<sup>-1</sup> (6.2%), respectively. This shows that the effect of the liquid desiccant inlet temperature on the performance of the dehumidifier is very small. Since the liquid desiccant is cooled by the evaporation of the water in the exhaust channel, its inlet temperature has a negligible effect on the change of the supply air humidity ratio and enthalpy. This will be shown clearly in ‘Contours of temperature and humidity ratio in the supply channel’.

#### Effect of liquid desiccant concentration

Figure 12 shows the supply air humidity ratio change,  $\Delta\omega_s$ , and the supply air enthalpy change,  $\Delta h_s$ , as functions of the liquid desiccant concentration,  $C_{LD,in}$ , for all 10 flow



**Fig. 11** The effect of liquid desiccant inlet temperature,  $T_{LD,in}$ , on **a, b** the humidity ratio change of the supply air and **c, d** the enthalpy change of the supply air for the 10 different flow arrangements of the 4-fluid dehumidifier

arrangements. Increasing the liquid desiccant concentration from 0.32 to 0.46 increases the change in supply air humidity ratio and enthalpy by about  $4.8 \text{ g kg}^{-1}$  (108%) and  $9.3 \text{ kJ kg}^{-1}$  (70.5%), respectively. When the liquid desiccant temperature is fixed, an increase in its concentration leads to a decrease in the vapor pressure of the air that is in equilibrium with it in the supply channel. The lower the vapor pressure, the higher the mass transfer potential. Therefore, increasing the liquid desiccant concentration leads to an increase in the supply air humidity ratio change.

#### Effect of liquid desiccant flow rate

Figure 13 shows the supply air humidity ratio change,  $\Delta\omega_s$ , and the supply air enthalpy change,  $\Delta h_s$ , as functions of

the liquid desiccant flow rate,  $v_{LD}$ , for all 10 flow arrangements. The plots of  $\Delta\omega_s$  and  $\Delta h_s$  are almost horizontal, that is, the flow rate of the liquid desiccant has very small effect on the performance of the dehumidifiers, which is in agreement with the experimental results [11]. Increasing the liquid desiccant flow rate from 6 to  $20 \text{ mL min}^{-1}$  increases the change in supply air humidity ratio and enthalpy by about  $0.04 \text{ g kg}^{-1}$  (0.6%) and  $0.2 \text{ kJ kg}^{-1}$  (1%), respectively. Given the use of membranes in the supply channels, the mass flow rate of the liquid desiccant relative to the supply air and exhaust air mass flow rates is very small, their ratio ranges from 3 to 25%. The small thermal mass of the liquid desiccant leads to a large change in its temperature along the dehumidifier, this is shown in ‘Contours of temperature and humidity ratio in the supply

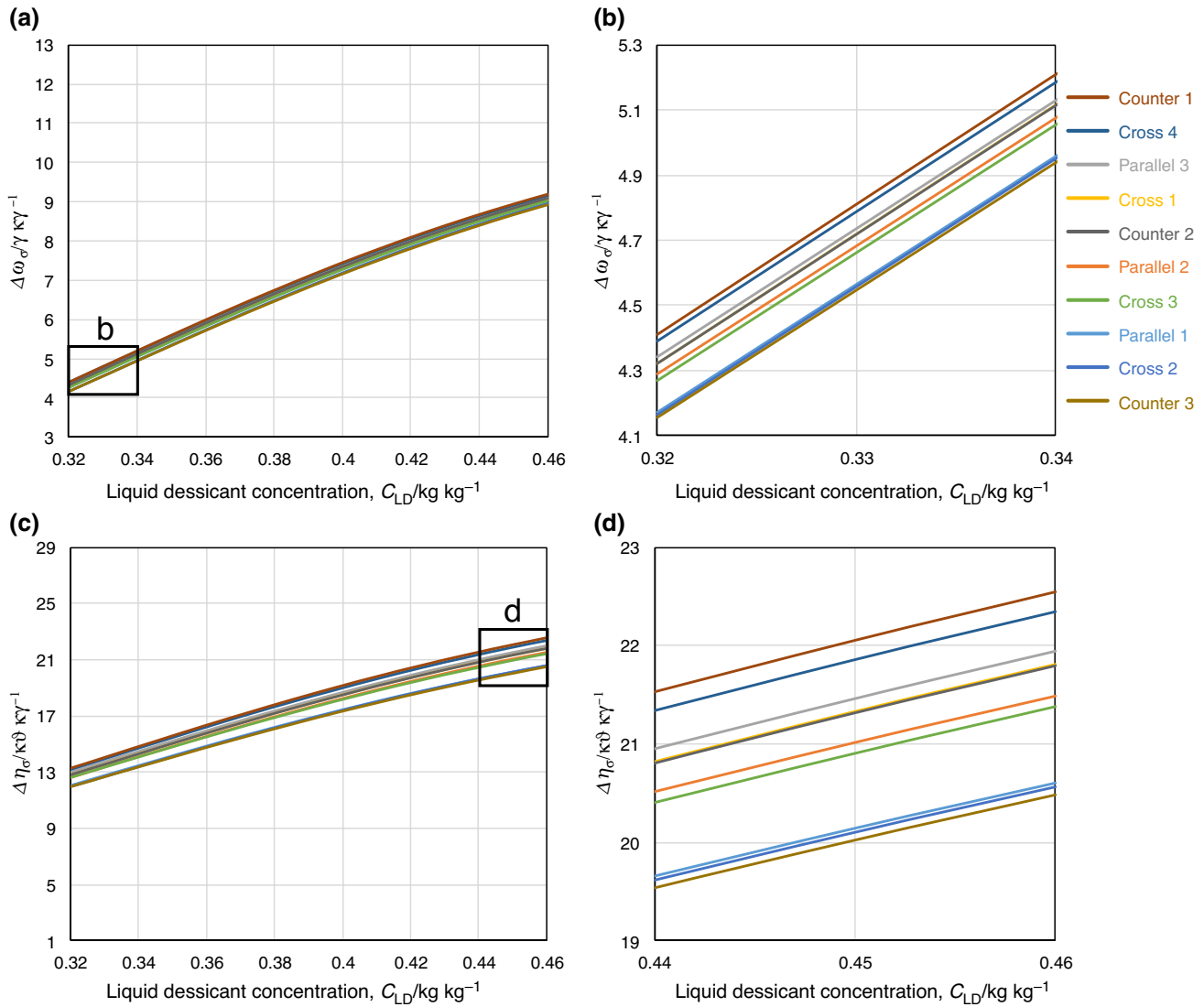


**Fig. 12** The effect of liquid desiccant concentration,  $C_{LD,in}$ , on **a, b** the humidity ratio change of the supply air and **c, d** the enthalpy change of the supply air for the 10 different flow arrangements of the 4-fluid dehumidifier

channel', minimizing its effect on the outlet conditions of the dehumidifier.

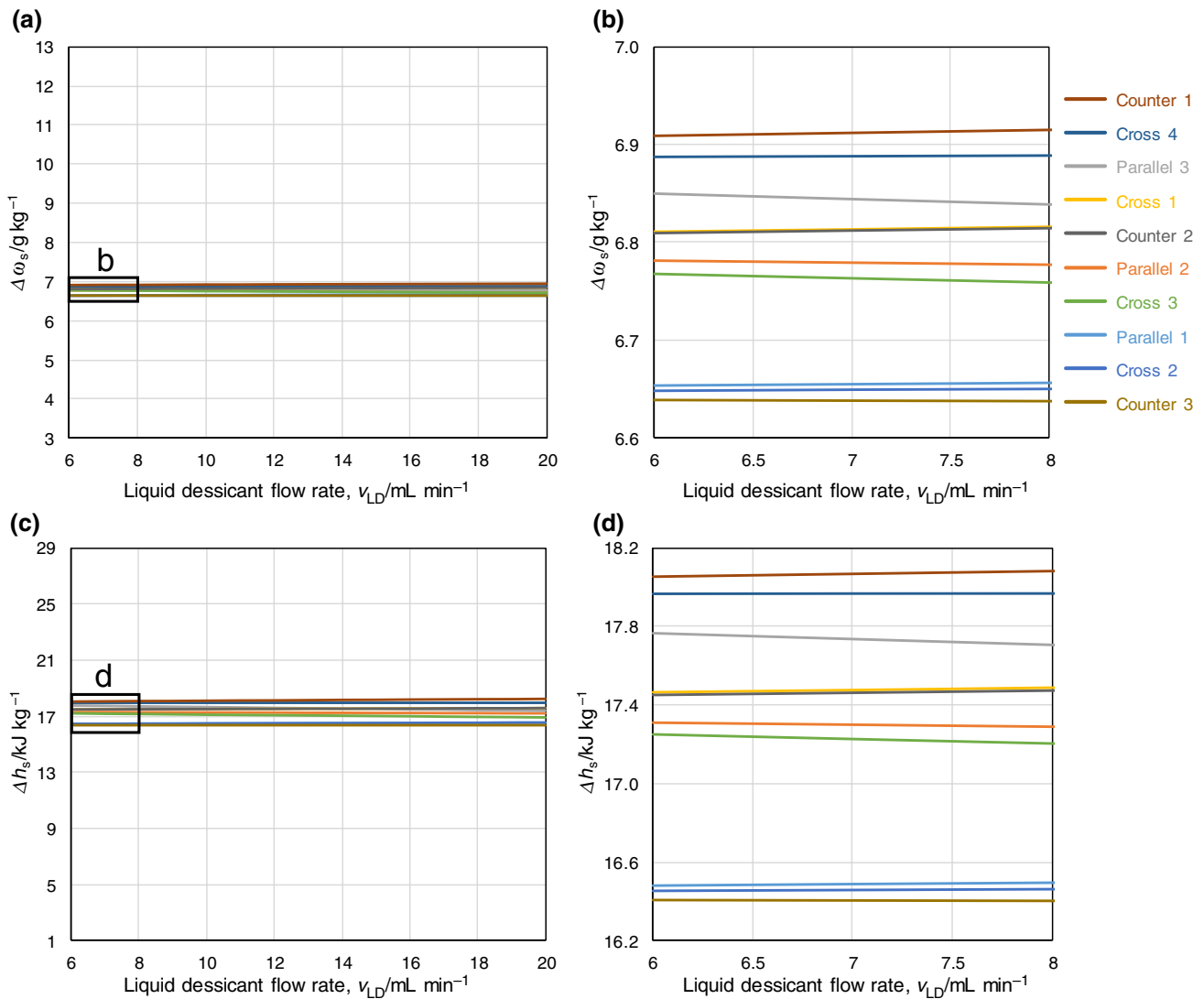
### Effect of supply air mass flow rate

Figure 14 shows the supply air humidity ratio change,  $\Delta\omega_s$ , and the supply air enthalpy change,  $\Delta h_s$ , as functions of the supply air mass flow rate,  $\dot{m}_s$ , for all 10 flow arrangements. Increasing the supply air mass flow rate from 2 to 8 g s<sup>-1</sup> reduces the change in supply air humidity ratio and enthalpy by about 5.3 g kg<sup>-1</sup> (54%) and 15.2 kJ kg<sup>-1</sup> (56.4%), respectively. As the supply air mass flow rate increases, the air flows faster in the supply channel, reducing the contact time between the air and the liquid

desiccant, which decreases the absorption of moisture from the supply air, leading to lower supply air humidity ratio and enthalpy change.

### Effect of exhaust to supply air mass flow rate ratio

Figure 15 shows the supply air humidity ratio change,  $\Delta\omega_s$ , and the supply air enthalpy change,  $\Delta h_s$ , as functions of the exhaust to supply air mass flow rate ratio,  $r$ , for all 10 flow arrangements. Increasing the exhaust to supply air mass flow rate ratio from 0 to 1, increases the change in supply air humidity ratio and enthalpy by about 4.2 g kg<sup>-1</sup> (134%) and 19.4 kJ kg<sup>-1</sup> (1830%), respectively. Increasing  $r$  from 0–0.2, leads to a sharp increase in the performance of the



**Fig. 13** The effect of liquid desiccant flow rate,  $v_{LD,in}$ , on **a, b** the humidity ratio change of the supply air and **c, d** the enthalpy change of the supply air for the 10 different flow arrangements of the 4-fluid dehumidifier

dehumidifiers. While this increase in performance almost flattens with further increase in  $r$ . The reason for this behavior can be explained as follows. The exhaust channel is the heat sink of the system. The higher the amount of air in the exhaust channel, the more cooling is provided to the supply channel, resulting in a decrease in the supply air and liquid desiccant temperatures. As pointed out before, the lower the temperature of the liquid desiccant along the dehumidifier, the higher the mass transfer potential, which lead to an increase in the supply air humidity ratio and enthalpy change.

### Contours of temperature and humidity ratio in the supply channel

Using the inlet conditions of test 8 specified in Table 2, the contours of temperature and humidity ratio of the airstream in the supply channel for all 10 flow arrangements obtained using the two-dimensional model are shown in Figs. 16 and 17, respectively. The supply air inlet temperature and humidity ratio are  $35^\circ\text{C}$  and  $18.6 \text{ g kg}^{-1}$ , respectively. The length and width of the channels are 0.4 m. The contours demonstrate the importance of using a two-dimensional model. Referring to Fig. 1, where the 10 flow arrangements are illustrated, it can be seen that there is two-dimensional variation in the temperature and humidity ratio contours in the flow arrangements when at least one of the fluid streams is perpendicular to the other streams.



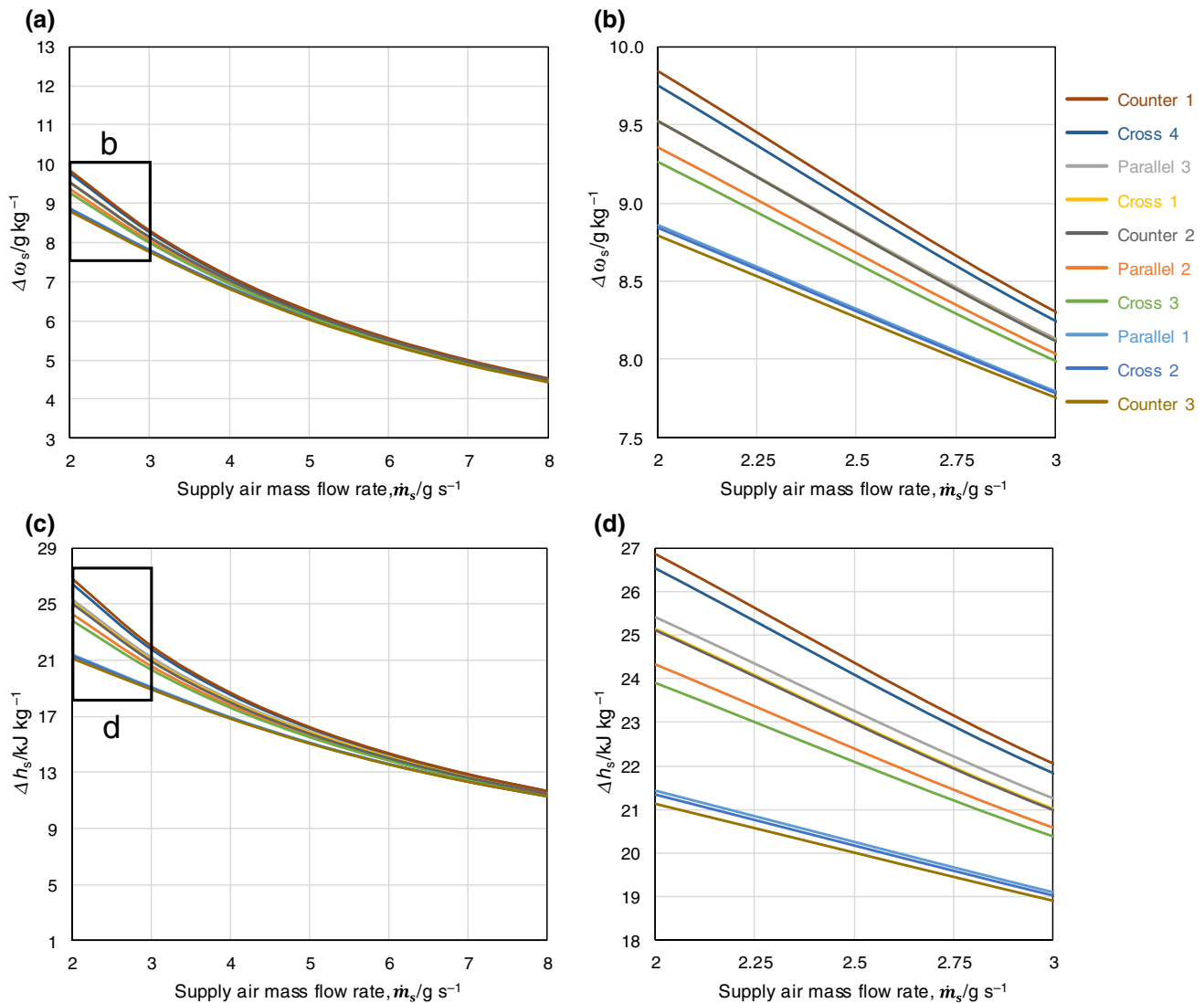


**Fig. 14** The effect supply air mass flow rate,  $\dot{m}_s$ , on **a, b** the humidity ratio change of the supply air and **c, d** the enthalpy change of the supply air for the 10 different flow arrangements of the 4-fluid dehumidifier

### Temperature and humidity ratio distribution in the counter 1 and 3 flow arrangements

Given that the dehumidifier's flow arrangements counter 1 and 3 have the highest and lowest performance, respectively, the distribution of the fluids temperature and humidity ratio along the dehumidifiers are analyzed. The temperature distribution of the supply air, exhaust air, liquid desiccant, and water film along the dehumidifiers with flow arrangements counter 1 and 3 are shown in Fig. 18a and c. The test 8 conditions from Table 2 are used as the inlet conditions. The arrows in the figure indicate the direction of the supply and exhaust air flow in the channels.

The supply air enters the dehumidifiers at 35 °C and exits at 34.6 °C from the counter 1 flow arrangement while it exits at 35.6 °C from the counter 3 flow arrangement. The highest temperature difference between the supply and exhaust air streams in the counter 1 flow arrangement reaches about 4 °C at about 60% of the width. While the highest temperature difference between the supply and exhaust air streams in the counter 3 flow arrangement reaches about 2.2 °C at about 40% of the width.

It can be seen that the liquid desiccant temperature variation along the width for both flow arrangements follows the trend of the water film since it is losing heat to it. Here, the negligible effect of the liquid desiccant inlet temperature and flow rate can be seen. The liquid desiccant's temperature

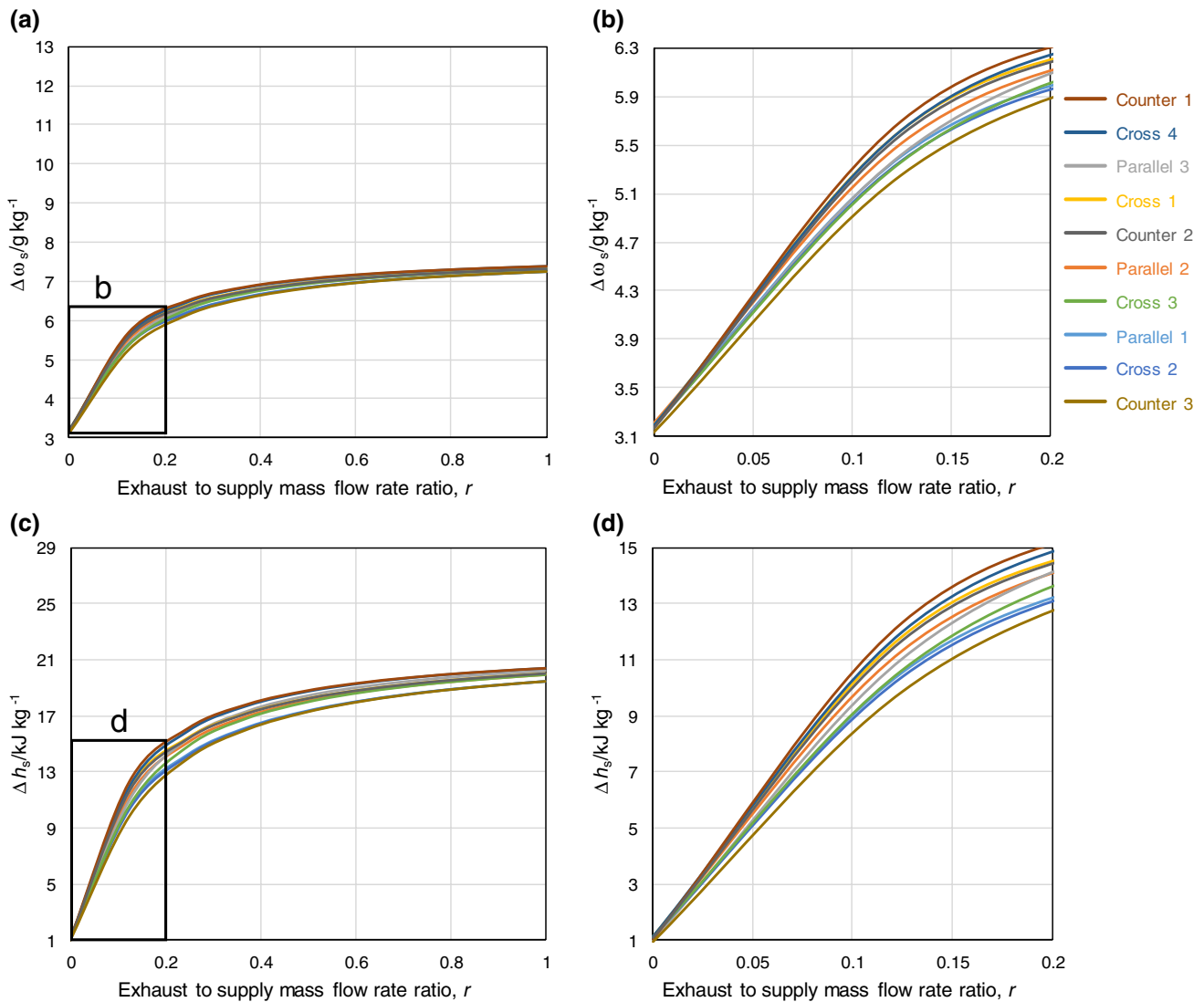


**Fig. 15** The effect exhaust to supply air mass flow rate ratio,  $r$ , on **a, b** the humidity ratio change of the supply air and **c, d** the enthalpy change of the supply air for the 10 different flow arrangements of the 4-fluid dehumidifier

changes sharply after passing about 5% (from 100 to 95%) of the width.

Figure 18b and d shows the humidity ratio distribution of the supply air,  $\omega_s$ , exhaust air,  $\omega_e$ , air in equilibrium with the liquid desiccant film,  $\omega_{LD}$ , and air in equilibrium with the water film,  $\omega_{wF}$ , along the dehumidifiers width with flow arrangements counter 1 and 3. The supply air enters

the dehumidifiers at a humidity ratio of  $18.6 \text{ g kg}^{-1}$  and exits at  $11.67 \text{ g kg}^{-1}$  from the counter 1 flow arrangement while it exits at  $11.96 \text{ g kg}^{-1}$  from the counter 3 flow arrangement. In both flow arrangements, the exhaust air humidity ratio increases along the direction of the flow and exits at a saturation state.

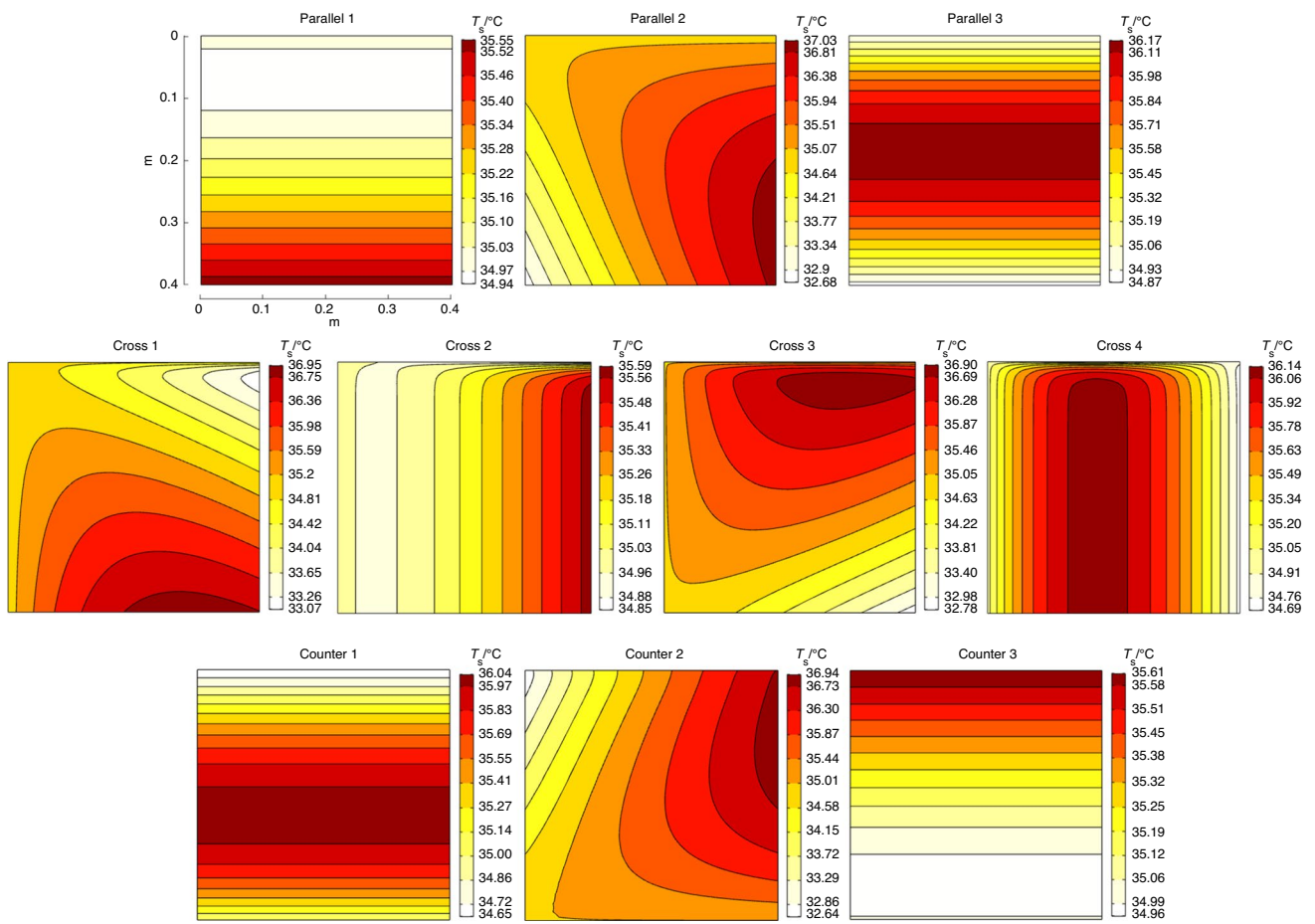


Fig. 16 Contours of temperature of the airstream in the supply channel for all 10 flow arrangements

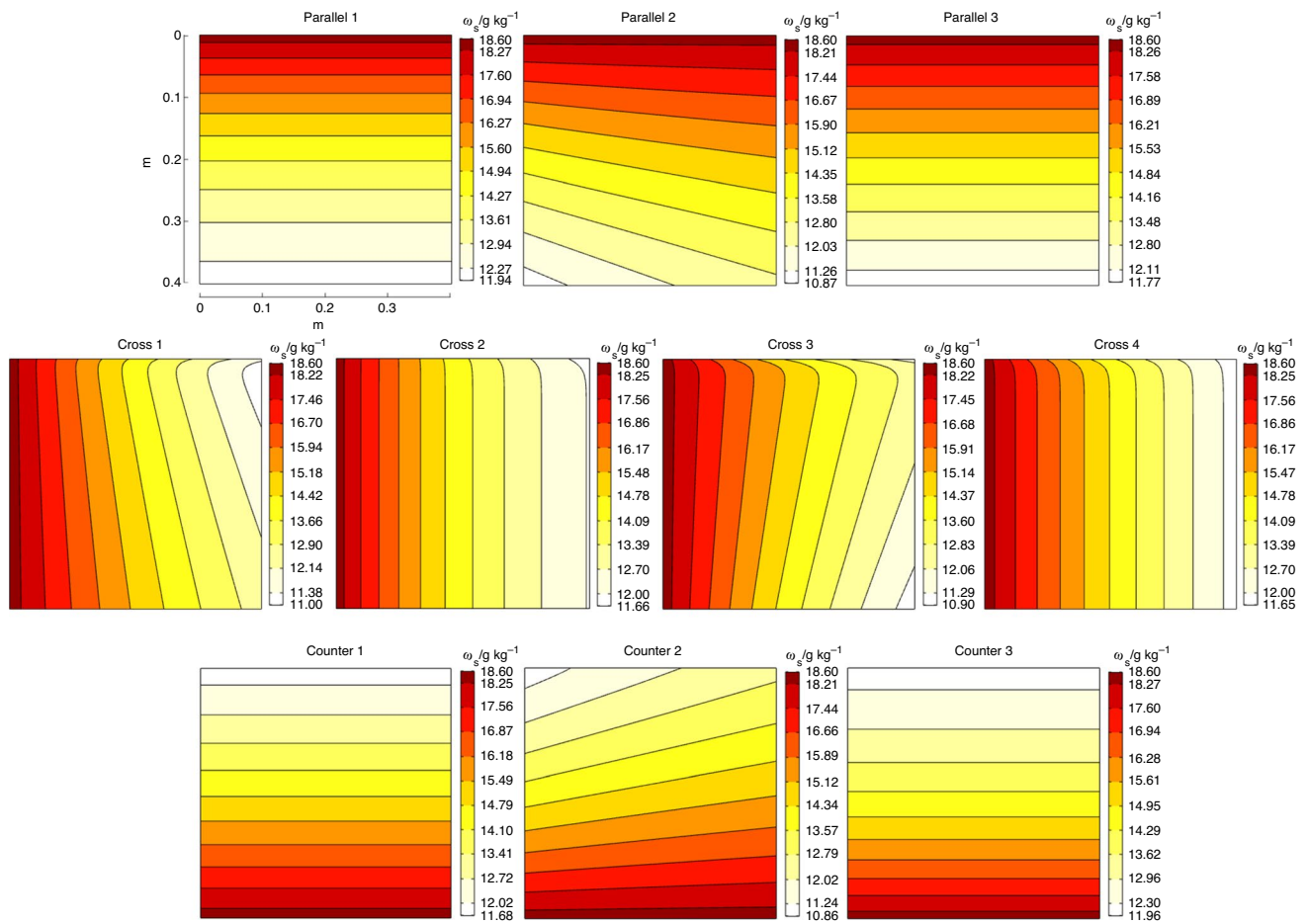
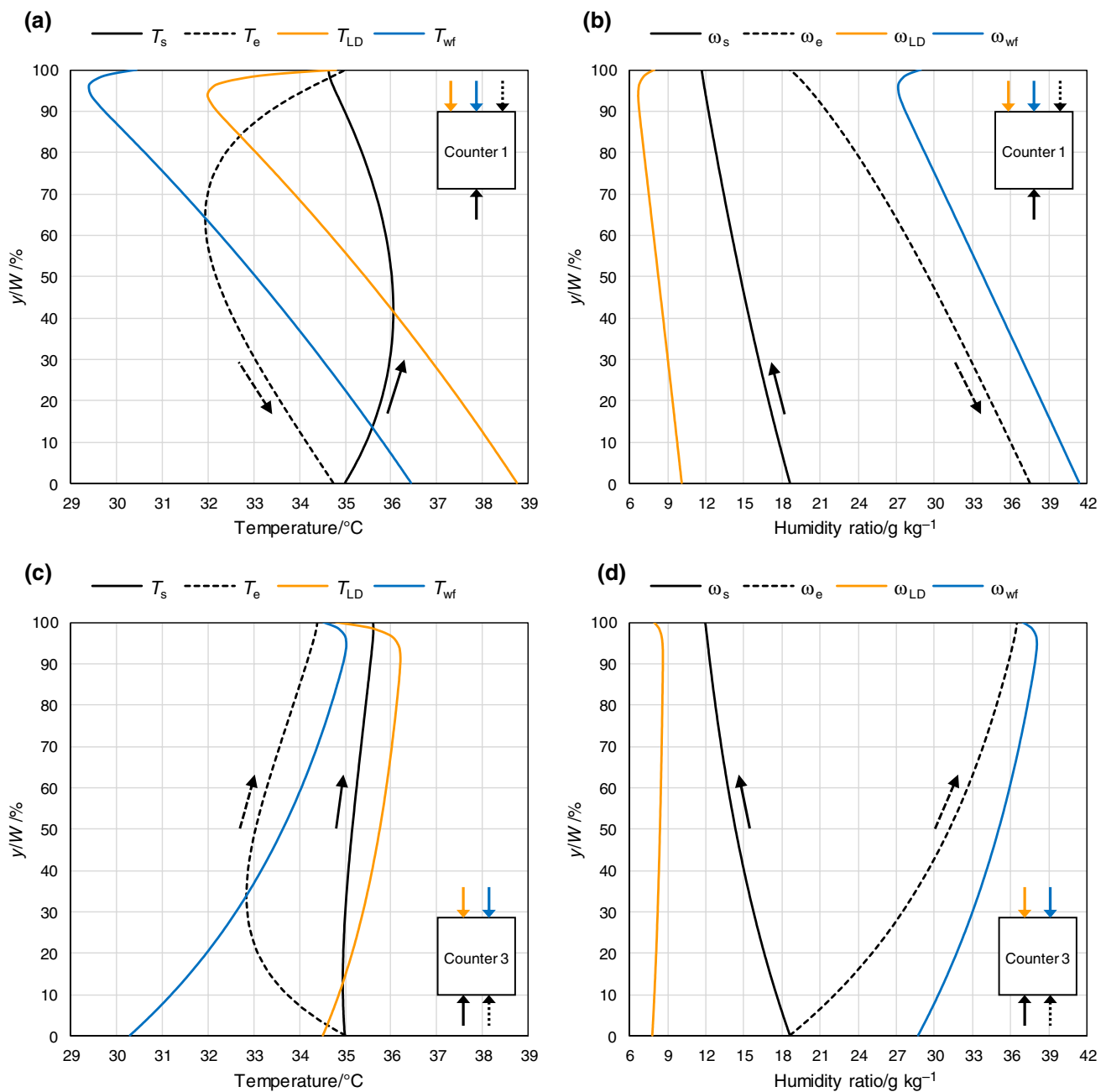


Fig. 17 Contours of humidity ratio of the airstream in the supply channel for all 10 flow arrangements



**Fig. 18** The variation of **a** temperature and **b** humidity ratio of the 4 fluids in the counter-flow 1 dehumidifier. The variation of **c** temperature and **d** humidity ratio of the 4 fluids in the counter-flow 3 dehumidifier

### Conclusions

In this study, 10 different flow arrangements of 4-fluid liquid desiccant dehumidifiers were compared in terms of the supply air humidity ratio change and supply air enthalpy change. The comparison was performed using a 2D numerical model of the heat and mass transfer in the dehumidifier, which was validated against experimental measurements from literature. The main conclusions of this study are as follows:

- The optimum performance (maximum supply air humidity ratio and enthalpy decrease) was obtained by the dehumidifier’s flow arrangement counter 1, in which the supply air is in counter-flow with the liquid desiccant and the exhaust air.
- The lowest performance (minimum supply air humidity ratio and enthalpy decrease) was obtained by the dehumidifier’s flow arrangement counter 3, in which the supply air is in counter-flow with the liquid desiccant and in parallel-flow with the exhaust air.

- The maximum difference between the highest and lowest performing dehumidifier's flow arrangements in terms of the supply air humidity ratio decrease was 4.3%, while it was 10.5% in terms of the supply air enthalpy decrease.
- The flow direction of the supply and exhaust air with respect to each other has more effect on the performance than the flow direction of the supply and liquid desiccant with respect to each other.
- The liquid desiccant inlet temperature and flow rate have negligible effect on the performance of the dehumidifier in all 10 flow arrangements. While increasing the liquid desiccant concentration improves the performance of the dehumidifier.

**Acknowledgements** This work was supported by the Qatar National Research Fund [Grant Number NPRP11S-0114-180295]. The contents of this work are solely the responsibility of the authors and do not necessarily represent the official views of the Qatar National Research Fund.

**Author contributions** AP: conceptualization, methodology, software, formal analysis, investigation, writing—original draft, writing—review & editing, visualization. SG: writing—review & editing, funding acquisition.

**Funding** The open access publication of this article was funded by Qatar National Library.

## Declarations

**Conflict of interest** The authors have no relevant financial or non-financial interests to disclose.

**Open Access** This article is licensed under a Creative Commons Attribution 4.0 International License, which permits use, sharing, adaptation, distribution and reproduction in any medium or format, as long as you give appropriate credit to the original author(s) and the source, provide a link to the Creative Commons licence, and indicate if changes were made. The images or other third party material in this article are included in the article's Creative Commons licence, unless indicated otherwise in a credit line to the material. If material is not included in the article's Creative Commons licence and your intended use is not permitted by statutory regulation or exceeds the permitted use, you will need to obtain permission directly from the copyright holder. To view a copy of this licence, visit <http://creativecommons.org/licenses/by/4.0/>.

## References

1. Isaac M, van Vuuren DP. Modeling global residential sector energy demand for heating and air conditioning in the context of climate change. *Energy Policy*. 2009;37:507–21. <https://doi.org/10.1016/j.enpol.2008.09.051>.
2. IEA. World Energy Outlook 2018. Paris: OECD; 2018. <https://doi.org/10.1787/weo-2018-en>.
3. Esmaeilzadeh A, Silakhori M, Nik Ghazali NN, Metselaar HSC, Bin Mamat A, Naghavi Sanjani MS, et al. Thermal performance and numerical simulation of the 1-pyrene carboxylic-acid functionalized graphene nanofluids in a sintered wick heat pipe. *Energies*. 2020. <https://doi.org/10.3390/en13246542>.
4. Naghavi MS, Esmaeilzadeh A, Singh B, Ang BC, Yoon TM, Ong KS. Experimental and numerical assessments of underlying natural air movement on PV modules temperature. *Sol Energy*. 2021;216:610–22. <https://doi.org/10.1016/j.solener.2021.01.007>.
5. Lowenstein A, Slayzak S, Kozubal E. A zero carryover liquid-desiccant air conditioner for solar applications. In: Am Sol Energy Soc—Sol 2006 35th ASES Annu Conf, 31st ASES Natl Passiv Sol Conf, 1st ASES Policy Mark Conf, ASME Sol Energy Div Int Sol Energy Conf. 2006;3:1396–406.
6. Bansal P, Jain S, Moon C. Performance comparison of an adiabatic and an internally cooled structured packed-bed dehumidifier. *Appl Therm Eng*. 2011;31:14–9. <https://doi.org/10.1016/j.applthermaleng.2010.06.026>.
7. Abdel-Salam MRH, Besant RW, Simonson CJ. Design and testing of a novel 3-fluid liquid-to-air membrane energy exchanger (3-fluid LAMEE). *Int J Heat Mass Transf*. 2016;92:312–29. <https://doi.org/10.1016/j.ijheatmasstransfer.2015.08.075>.
8. Woods J, Kozubal E. On the importance of the heat and mass transfer resistances in internally-cooled liquid desiccant dehumidifiers and regenerators. *Int J Heat Mass Transf*. 2018;122:324–40. <https://doi.org/10.1016/j.ijheatmasstransfer.2018.01.111>.
9. Xiao L, Yang M, Yuan WZ, Huang SM. Performance characteristics of a novel internally-cooled plate membrane liquid desiccant air dehumidification system. *Appl Therm Eng*. 2020;172: 115193. <https://doi.org/10.1016/j.applthermaleng.2020.115193>.
10. Saman WY, Alizadeh S. Modelling and performance analysis of a cross-flow type plate heat exchanger for dehumidification/cooling. *Sol Energy*. 2001;70:361–72. [https://doi.org/10.1016/S0038-092X\(00\)00148-1](https://doi.org/10.1016/S0038-092X(00)00148-1).
11. Woods J, Kozubal E. A desiccant-enhanced evaporative air conditioner: Numerical model and experiments. *Energy Convers Manage*. 2013;65:208–20. <https://doi.org/10.1016/j.enconman.2012.08.007>.
12. Jafarian H, Sayyaadi H, Torabi F. Numerical modeling and comparative study of different membrane-based liquid desiccant dehumidifiers. *Energy Convers Manage*. 2019;184:735–47. <https://doi.org/10.1016/j.enconman.2019.01.099>.
13. Liu XH, Chang XM, Xia JJ, Jiang Y. Performance analysis on the internally cooled dehumidifier using liquid desiccant. *Build Environ*. 2009;44:299–308. <https://doi.org/10.1016/j.buildenv.2008.03.009>.
14. Liu J, Liu X, Zhang T. Performance comparison and exergy analysis of different flow types in internally-cooled liquid desiccant dehumidifiers (ICDs). *Appl Therm Eng*. 2018;142:278–91. <https://doi.org/10.1016/j.applthermaleng.2018.07.006>.
15. Li W, Yao Y. Thermodynamic analysis of internally-cooled membrane-based liquid desiccant dehumidifiers of different flow types. *Int J Heat Mass Transf*. 2021;166: 120802. <https://doi.org/10.1016/j.ijheatmasstransfer.2020.120802>.
16. Li W, Yao Y. Performance analysis of different flow types of internally-cooled membrane-based liquid desiccant dehumidifiers. *Energy*. 2021. <https://doi.org/10.1016/j.energy.2021.120597>.
17. Guan B, Liu X, Zhang T, Liu J. Optimal flow type in internally-cooled liquid-desiccant system driven by heat pump: component level vs. System level. *Appl Therm Eng*. 2021. <https://doi.org/10.1016/j.applthermaleng.2020.116208>.
18. Pakari A, Ghani S. Comparison of 1D and 3D heat and mass transfer models of a counter flow dew point evaporative cooling system: numerical and experimental study Étude comparative numérique et expérimentale de modèles de transfert de chaleur



- et de masse 1D et 3D d'un sys. *Int J Refrig.* 2019;99:114–25. <https://doi.org/10.1016/j.ijrefrig.2019.01.013>.
19. Pakari A, Ghani S. Regression models for performance prediction of counter flow dew point evaporative cooling systems. *Energy Convers Manage.* 2019;185:562–73. <https://doi.org/10.1016/j.enconman.2019.02.025>.
  20. Cengel Y, Boles M. *Thermodynamics an engineering approach*. 5th ed. New York: McGraw-Hill Companies, Inc.; 2006.
  21. Conde MR. Properties of aqueous solutions of lithium and calcium chlorides: formulations for use in air conditioning equipment design. *Int J Therm Sci.* 2004;43:367–82. <https://doi.org/10.1016/j.jthermalsci.2003.09.003>.
  22. Buck AL. New equations for computing vapor pressure and enhancement factor. *J Appl Meteorol.* 1981;20:1527–32. [https://doi.org/10.1175/1520-0450\(1981\)020%3c1527:NEFCVP%3e2.0.CO;2](https://doi.org/10.1175/1520-0450(1981)020%3c1527:NEFCVP%3e2.0.CO;2).
  23. Buck AL. CR-1A HYGROMETER OPERATING MANUAL. 2012.
  24. Sharqawy MH, Lienhard VJH, Zubair SM. The thermophysical properties of seawater: a review of existing correlations and data accessed thermophysical properties of seawater: A review of existing correlations and data. *Desalin Water Treat.* 2010;16:354–80. <https://doi.org/10.5004/dwt.2010.1079>.
  25. Shah RK, London AL. Chapter VI—parallel plates. In: Shah RK, London AL, editors. *Laminar flow forced convect. Ducts*. Cambridge: Academic Press; 1978. p. 153–95. <https://doi.org/10.1016/B978-0-12-020051-1.50011-5>.

**Publisher's Note** Springer Nature remains neutral with regard to jurisdictional claims in published maps and institutional affiliations.